Stem Cell Reports
Article

ISSCR

OPEN ACCESS

Age-related pathological impairments in directly reprogrammed dopaminergic neurons derived from patients with idiopathic Parkinson's disease

Janelle Drouin-Ouellet,[1,6,*] Emilie M. Legault,[1,6] Fredrik Nilsson,[2] Karolina Pircs,[2] Julie Bouquety,[1] Florence Petit,[1] Shelby Shrigley,[2] Marcella Birtele,[2] Maria Pereira,[2] Petter Storm,[2] Yogita Sharma,[2] Andreas Bruzelius,[2] Romina Vuono,[3,4] Malin Kele,[5] Thomas B. Stoker,[3] Daniella Rylander Ottosson,[2] Anna Falk,[5] Johan Jakobsson,[2] Roger A. Barker,[3] and Malin Parmar[2,*]

[1]Faculty of Pharmacy, Université de Montréal, Montreal, QC H3T 1J4, Canada
[2]Department of Experimental Medical Science, Wallenberg Neuroscience Center, Division of Neurobiology and Lund Stem Cell Center, Lund University, BMC A11 and B10, S-221 84 Lund, Sweden
[3]Wellcome-MRC Cambridge Stem Cell Institute & John van Geest Centre for Brain Repair, Department of Clinical Neurosciences, University of Cambridge, Forvie Site, Cambridge CB2 0PY, UK
[4]Medway School of Pharmacy, University of Kent, Chatham Maritime, Chatham ME4 4TB, UK
[5]Department of Neuroscience, Karolinska institutet, Stockholm, Sweden
[6]These authors contributed equally
*Correspondence: janelle.drouin-ouellet@umontreal.ca (J.D.-O.), malin.parmar@med.lu.se (M.P.)
https://doi.org/10.1016/j.stemcr.2022.08.010

SUMMARY

We have developed an efficient approach to generate functional induced dopaminergic (DA) neurons from adult human dermal fibroblasts. When performing DA neuronal conversion of patient fibroblasts with idiopathic Parkinson's disease (PD), we could specifically detect disease-relevant pathology in these cells. We show that the patient-derived neurons maintain age-related properties of the donor and exhibit lower basal chaperone-mediated autophagy compared with healthy donors. Furthermore, stress-induced autophagy resulted in an age-dependent accumulation of macroautophagic structures. Finally, we show that these impairments in patient-derived DA neurons leads to an accumulation of phosphorylated alpha-synuclein, the classical hallmark of PD pathology. This pathological phenotype is absent in neurons generated from induced pluripotent stem cells from the same patients. Taken together, our results show that direct neural reprogramming can be used for obtaining patient-derived DA neurons, which uniquely function as a cellular model to study age-related pathology relevant to idiopathic PD.

INTRODUCTION

Parkinson's disease (PD) is a neurodegenerative disorder that has a major pathology within the midbrain dopaminergic (DA) neurons and involves the aggregation of the misfolded protein alpha-synuclein (αSYN). How the disease arises and develops is currently unknown and no cure exists. There is an urgent need for better treatments and disease modifying therapies, but their development is hampered by a poor understanding of the pathogenesis of PD and lack of appropriate model systems, in particular ones that capture age, the biggest risk factor for developing this condition.

To better recapitulate disease relevant features and age, we have established a protocol for making induced neurons (iNs) that can be directly generated from adult human dermal fibroblasts (aHDFs). This type of direct neural conversion offers several advantages. In particular, such cells retain many important aspects of the aging signatures of the starting fibroblasts, including age-related changes in the epigenetic clock, the transcriptome and microRNAs, the reactive oxygen species level, DNA damage and telomeres length, as well as in their metabolic profile and mitochondrial defects (Huh et al., 2016; Kim et al., 2018; Mertens et al., 2015, 2021; Tang et al., 2017).

The idiopathic nature of most PD cases, coupled to the late age at onset, complicates the study of pathophysiology as it is challenging to design and interpret models of idiopathic PD. For example, animal models depend on toxin-induced mitochondrial damage or overexpression of αSYN at non-physiological levels (i.e., levels that exceed what is observed in idiopathic PD patients). Patient-derived induced pluripotent stem cells (iPSCs) are frequently used to study cellular features of PD (Brazdis et al., 2020; Lang et al., 2019) but fail to capture the age and epigenetic signatures of the patient (Lapasset et al., 2011; Mertens et al., 2015, 2021; Miller et al., 2013; Tang et al., 2017).

In this study, we investigated iNs using specific combinations of transcription factors and fate determinants without a pluripotent intermediate (Ambasudhan et al., 2011) as a mean to better recapitulate disease-relevant features of idiopathic PD. While it is possible to generate iNs with a DA-like phenotype (Caiazzo et al., 2011; Jiang et al., 2015; Li et al., 2019; Pereira et al., 2014; Pfisterer et al., 2011), current protocols are not efficient enough to

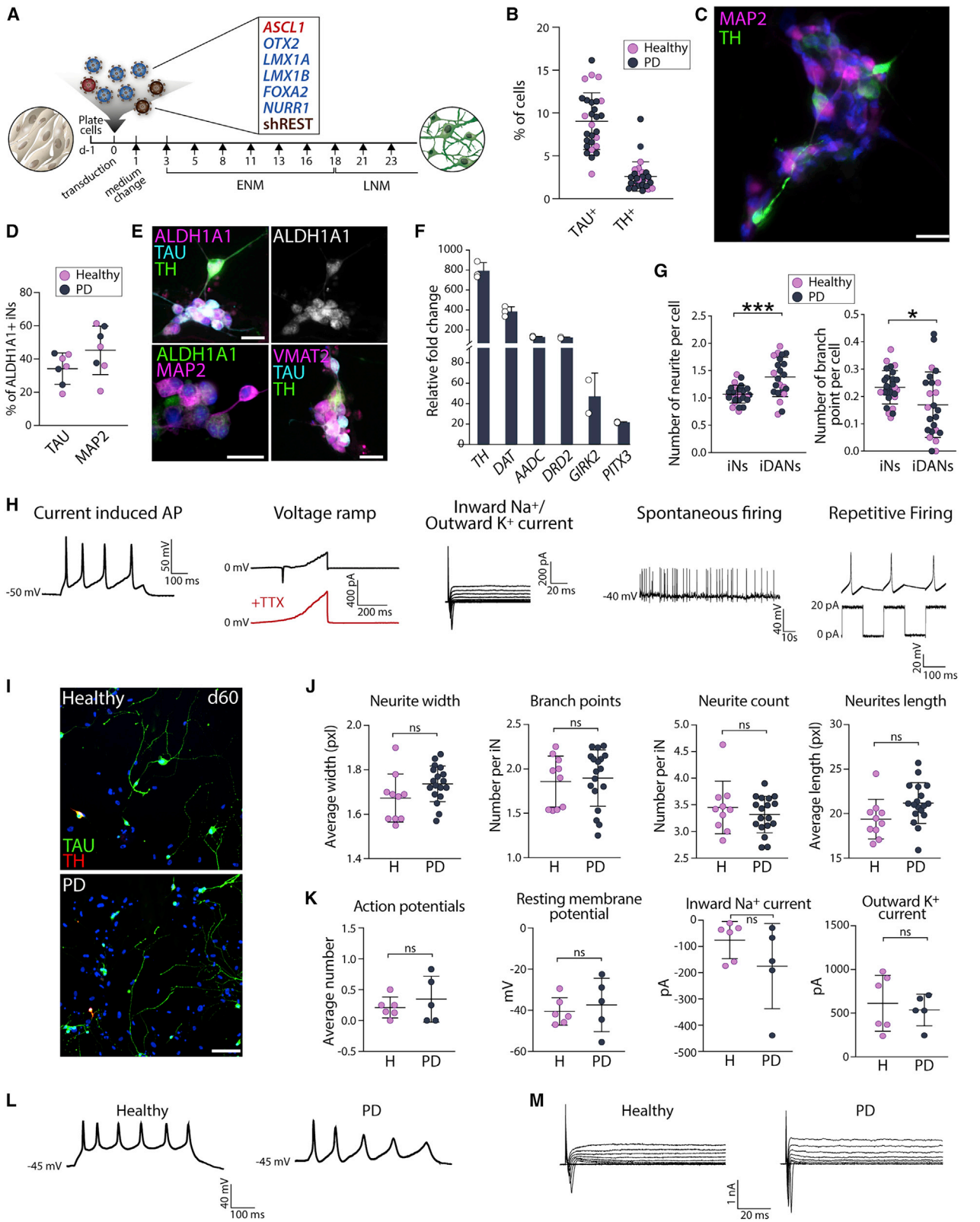

(legend on next page)

generate DA neurons from aHDFs of elderly donors in numbers required for further downstream experimental studies. Therefore, we first identified a combination of reprogramming factors that resulted in the efficient generation of subtype-specific and functional induced DA neurons (iDANs) when converting aHDFs from aged individuals. Subsequently, we used this protocol to convert iDANs from idiopathic PD patient-derived aHDFs as well as age- and sex-matched controls.

When analyzing the patient-derived neurons, we found stress-induced chaperone-mediated autophagy (CMA) and macroautophagy impairments in the idiopathic PD iNs but not in control iNs or in parental aHDFs of the patients. This type of pathology has previously only been captured in genetic PD variants using iPSC-based models (Sánchez-Danés et al., 2012; Schöndorf et al., 2014), and we hypothesized that the ability to do so in idiopathic PD iNs as reported here is related to maintenance of donor age in the iNs. To test this, we established iPSCs from a subset of the same patients. This analysis confirmed that fibroblast-derived iNs maintain expression of age-associated genes and express mature isoforms of TAU (4R), whereas iPSC-derived iNs do not. In line with this, we were able to detect αSYN pathology in directly converted patient-derived neurons but not in iPSC-generated patient-derived neurons. This study thus reports PD-associated phenotypes in directly converted neurons from patient aHDFs and provides a new model to study idiopathic forms of PD.

RESULTS

Generation of functional iDANs from aHDFs of adult donors

To enable a cell-based model of idiopathic PD using iNs with characteristics of aged DA neurons, we screened 10 different reprogramming factors (*Ascl1*, *Lmx1a*, *Lmx1b*, *Foxa2*, *Otx2*, *Nr4a2* (*Nurr1*), *SMARCA1*, *CNPY1*, *EN1*, *PAX8*) that were selected based on their (1) role during normal DA neurogenesis (Luo and Huang, 2016), (2) expression in the normal human fetal ventral midbrain (Nelander et al., 2013), (3) value in predicting functional DA differentiation from hPSCs (Kirkeby et al., 2017), and/or (4) role on midbrain-specific chromatin modeling (Metzakopian et al., 2015). All factors were expressed in combination with the knockdown of the RE1-silencing transcription factor (*REST*) according to our published protocol for high efficiency reprograming of aHDFs (Drouin-Ouellet et al., 2017). Three of the screened combinations gave rise to a significant proportion of tyrosine hydroxylase (TH)-expressing neurons: sh*REST*, *Ascl1*, *Lmx1a*, *Lmx1b*, *Foxa2*, *Otx2* (2.21% ± 2.02), sh*REST*, *Ascl1*, *Lmx1a*, *Lmx1b*, *Foxa2*, *Otx2*, *SMARCA1* (7.50% ± 3.55%), and sh*REST*, *Ascl1*, *Lmx1a*, *Lmx1b*, *Foxa2*, *Otx2*, *Nr4a2* (Figures 1A and S1A). The best TH-positive cell yield was obtained with the last combination, which gave rise to up to 70.3% ± 0.3% of cells expressing the neuronal marker TAU, of which 16.1% ± 2.01% also expressed TH (Figure S1A),

Figure 1. Generation of iDANs from Parkinson's disease and heathy donor lines

(A) Reprogramming iDANs from adult fibroblasts.

(B) Quantification of TAU-positive and TH-positive cells (mean average of 2,575 TAU-positive and 32 TH-positive cells assessed per line, n = 28 lines). Data are expressed as mean ± the SD.

(C) TAU-positive and TH-positive iDANs. Cells are counterstained with DAPI (in blue). Scale bar, 25 μm.

(D) Quantification of ALDH1A1 and TAU or MAP2 double-positive cells (mean average of 1,652 TAU-positive and 1,258 MAP2-positive cells assessed per well from four replicates per line, n = 7 lines (lines #4, #8, #9, #10, #26, #27, and #28). Data are expressed as mean ± the SD.

(E) TAU-positive, MAP2-positive, and TH-positive iNs and iDANs expressing ALDH1A1 and VMAT2. Cells are counterstained with DAPI (in blue). Scale bars, 25 μm.

(F) Gene expression quantification of DA genes relative to parental fibroblast levels (from two to three well replicates [white dots] from line #2). Data are expressed as mean ± the SD.

(G) Quantification of the neurite profile in TAU-positive and TH-negative (iNs) versus TAU and TH double-positive cells (iDANs) from healthy and Parkinson's disease lines (mean average of 2,575 TAU-positive and 32 TH-positive cells assessed per line, n = 28 lines). Two-tailed unpaired t test with Welch's correction: ***p = 0.0004, df = 30.82; *p = 0.0245, df = 32.94. Data are expressed as mean ± the SD.

(H) Patch clamp recordings of iDANs from line #2 (at day 65).

(I) Double TAU-positive and TH-positive H-iDANs and PD-iDANs at day 60. Scale bar, 100 μm.

(J) Quantification of the neurite profile in TAU-positive H-iNs and PD-iNs (experiment has been repeated independently three times, mean average of 2,142 TAU-positive cells assessed per line, n = 10 healthy and n = 18 Parkinson's disease lines). Data are expressed as mean ± the SD.

(K) Quantification of voltage-clamp recordings of evoked action potentials (n = 8–10 neurons per line, n = 5–6 lines per group), resting membrane potential of H-iNs and PD-iNs (n = 4–9 neurons per line, n = 5–6 lines per group), inward and outward currents (n = 4–9 neurons per line, n = 5–6 lines per group). Lines #1, #2, #4, #5, #6, #8, #13, #16, #17, #24, #28 were used for patch clamp experiments. Data are expressed as mean ± the SD.

(L) Voltage-clamp recordings of repetitive evoked action potentials.

(M) Representative traces of membrane sodium and potassium currents following voltage depolarization steps in H-iNs and PD-iNs. APs, action potentials; ns, not significant; TTX, tetrodotoxin.

with an average TAU purity of 9.1% ± 3.3% and TH purity of 2.6% ± 1.7% (Figures 1B and 1C) when reprogramming all lines used in the study (see Table 1), and showed robust upregulation of DA genes as measured by RT-qPCR (Figure S1B).

Further characterization of the iNs obtained using this reprogramming factor combination showed that, in addition to TH, 35.38% ± 9.05% of the TAU-positive and 45.20% ± 14.65% of the MAP2-positive cells were also expressing ALDH1A1 (Figure 1D), which is found in a subset of A9 DA neurons that are more vulnerable to loss in PD (Poulin et al., 2014), as well as VMAT2, a key DA neuronal marker (Figure 1E). Gene expression profiling of 76 neuronal genes relating to dopaminergic, glutamatergic, and GABAergic neuronal subtypes confirmed an upregulation of key genes related to DA patterning and identity (*FOXA1*, *OTX1*, *SHH*, *PITX3*), as well as DA synaptic function, including the receptors *DRD1* to *DRD5*; the DA transporter *SLC6A3* (*DAT*); the enzymes *DDC*, *MAOA*, and *ALDH1A1*; and the A9-enriched DA marker *KCNJ6* (*GIRK2*) (Figures 1F, S1C, and S1D). Thus the iDANs expressed the key markers of the AT-DAT^{high} subgroup of the DA sublineage as identified in Tiklová et al. (2019). Finally, to get a better idea of the identity of the cells that did not convert to iNs, we performed a triple staining using MAP2 to identify iNs, as well as GFAP and collagen 1 to identify potential glial cells and cells that remained fibroblasts. We observed that some MAP2-negative cells are expressing either collagen 1 or GFAP alone, or together (Figure S1E).

Morphologically, the iNs are quite immature at this stage (i.e., day 25–30), but high-throughput image acquisition analysis showed that TH-positive iNs express significantly more neurites compared with non-TH iNs but had significantly fewer branch points (Figure 1G). Patch-clamp electrophysiological recordings 65 days post transduction confirmed that the reprogrammed cells had functionally matured (Figure 1H). They were able to fire repetitive action potentials upon injection of current as well as exhibited inward-sodium, outward-potassium currents with depolarizing steps. When a continuous depolarizing voltage ramp was applied, inward currents were seen across the membrane and could be blocked by the neurotoxin tetrodotoxin, indicating an involvement of voltage-gated sodium channels in these currents. Without any injection of current or voltage, the cells displayed spontaneous firing, and 43.8% of iNs also showed rebound action potentials and/or pacemaker-like activity typical of mesencephalic DA neurons (Figure 1H). Based on this, we refer to the cells as iDANs.

Generation of functional iDANs from aHDFs of idiopathic Parkinson's disease patients

Using this new iDAN reprogramming method, we next converted aHDFs of 18 idiopathic PD patients and 10 age- and sex-matched healthy donors (Table 1). We found that the aHDFs obtained from PD patients reprogrammed at a similar efficiency to those obtained from healthy donors (Figure 1B) and displayed a similar neuronal morphological profile (Figures 1I and 1J). When measuring their functional properties using patch clamp electrophysiological recordings, we confirmed that iNs derived from healthy donors (H-iNs) and from PD patients (PD-iNs) displayed similar functionalities in terms of the number of current-induced action potentials, resting membrane potential, and the inward-sodium, outward-potassium currents (Figures 1K–1M).

PD-iDANs show altered chaperone-mediated autophagy

To assess the presence of age- and PD-related pathological impairments in iDANs derived from idiopathic PD patients, we focused on autophagy, a lysosomal degradation pathway that is important in cellular homeostasis and the efficiency of which decreases with age (Rubinsztein et al., 2011). We first looked for CMA alterations as this is one type of autophagy that has been suggested to be implicated in the pathophysiology of PD (Cuervo et al., 2004). During CMA, HSC70 recognizes soluble proteins carrying a KFERQ-like motif and guides them to the transmembrane LAMP2a receptor. Thereafter, the protein cargo is translocated into the lysosomal lumen and, as such, the level of LAMP2a determines the rate of CMA (Klionsky et al., 2016). To induce autophagy, cells were cultured under starvation conditions, which promotes the recycling of non-essential proteins and organelles for reuse (Klionsky et al., 2016). After validating that the starvation regimen had no impact on the number of neurons and induced changes in LAMP2a and HSC70 expression using western blot (WB) (Figures S2A–S2C), we assessed CMA expression using a high-content imaging approach, which allowed us to analyze cytoplasmic puncta in parental aHDFs, iNs (TAU positive and TH negative), and iDANs (TAU positive and TH positive) in a quantitative manner, and also to determine their subcellular location. When investigating this in parental aHDFs and PD-iNs at baseline and in the context of starvation using an antibody specific to the "a" isoform of LAMP2, we observed a slight reduction in LAMP2a-positive cytoplasmic puncta in healthy donors' parental aHDFs, which was also seen in PD patients' aHDFs, although this was not significant (Figures S2F and S2G). Moreover, we did not observe a difference in LAMP2a-positive cytoplasmic puncta in the neurites of TAU-positive iNs upon starvation in both H-iNs and PD-iNs (Figures S2J and S2K). However, when looking specifically at iDANs, we observed a lower number of LAMP2a-positive cytoplasmic puncta in the neurites at baseline in the PD-iDANs compared with H-iDANs, suggesting a lower

Table 1. Demographics, clinical, and genotype data of the study participants

Line ID	Group	Sex	Age at biopsy	MAPT haplotype	Age at onset (years)	Disease duration (years)	[a]UPDRS motor decline	[a]MMSE score decline	iPSC lines
1	healthy	M	69	H1/H1					
2	healthy	F	67	H1/H1					
3	healthy	M	80	H2/H2					
4	healthy	F	75	H1/H1					healthy 4
5	healthy	M	70	H1/H2					healthy 5
6	healthy	F	70	H1/H2					
7	healthy	M	71	H1/H1					
8	healthy	F	61	H1/H2					healthy 8
9	healthy	F	66	H2/H2					
10	healthy	F	58	H1/H1					
	ratio F:M/ mean ± SD	6:4	68.7 ± 6.3						
11	PD	M	56	H1/H1	34	23	−0.32	0	
12	PD	M	60	H1/H1	48	12	−0.43	0	
13	PD	F	77	H2/H2	65	12	1.48	0	
14	PD	F	67	H1/H1	56	12	0.76	−0.07	
15	PD	F	59	H1/H1	45	15	−1.39	0	
16	PD	F	80	H1/H2	69	11	0.39	−0.07	
17	PD	M	80	H2/H2	49	33	1.70	0	
18	PD	F	87	H1/H1	72	15	0.25	−0.12	
19	PD	F	77	H1/H1	56	24	−0.42	−0.25	
20	PD	M	75	H1/H1	63	13	−1.18	0	
21	PD	M	77	H1/H1	66	11	−1.68	0	
22	PD	F	71	H1/H1	62	14	0	−0.47	
23	PD	M	72	H1/H1	70	2	1.71	−0.44	
24	PD	M	81	H1/H1	76	6	1.88	0.14	
25	PD	F	44	H1/H1	40	5	−3.56	0.15	
26	PD	F	79	H1/H1	NA	NA	NA	NA	PD 26
27	PD	F	68	H1/H1	55	15	1.65	0	
28	PD	M	57	H1/H1	50	8	NA	NA	PD 28
	ratio F:M/mean ± SD	10:8	70.4 ± 11.2		57.4 ± 11.9	12.5 ± 7.1	0.05 ± 1.5	−0.07 ± 0.18	

MMSE, Mini-Mental State Examination; NA, not available; UPDRS, Unified Parkinson's Disease Rating Scale.
[a]Average rate of decline per year over a minimum of 2 years.

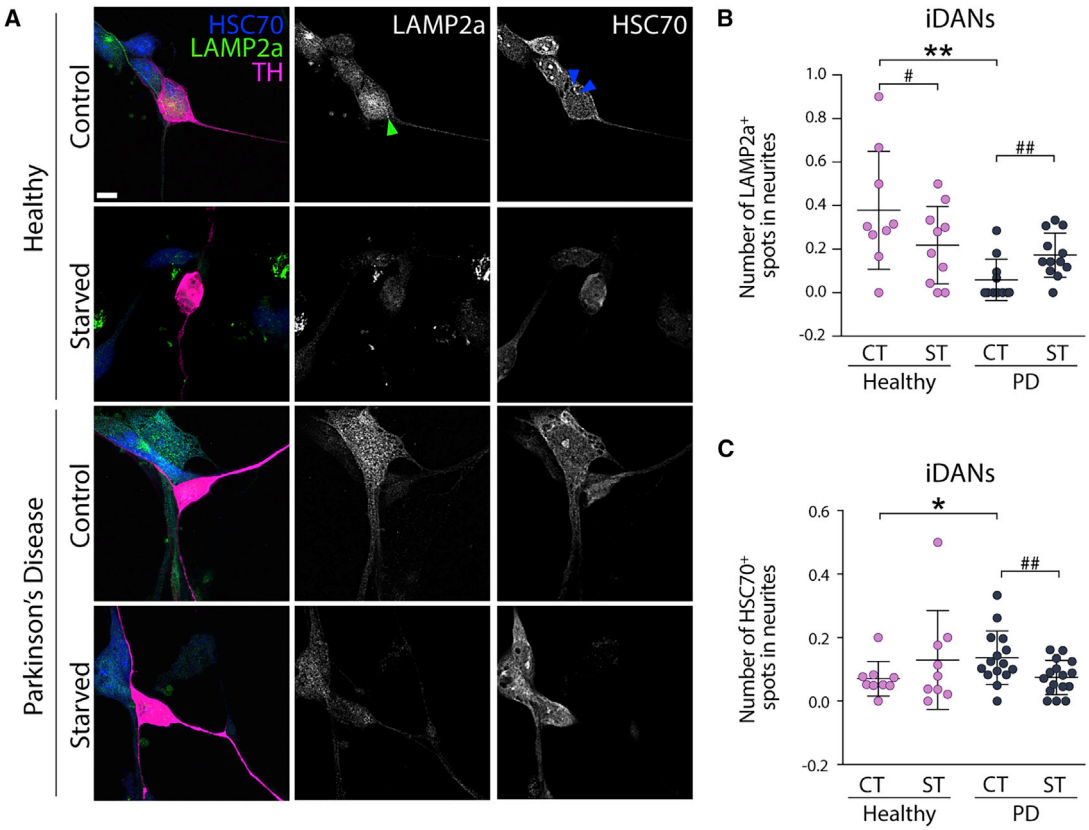

Figure 2. Chaperone-mediated autophagy impairment in PD-iDANs

(A) LAMP2a-positive dot expression and spot detection analysis of LAMP2a-positive (green arrowhead) and HSC70-positive (blue arrowheads) puncta in TH-positive iDANs. Scale bar, 10 μm.

(B) Quantification of LAMP2a-positive puncta in the neurites of TH-positive iDANs (mean average of 14 TH-positive cells assessed per line, n = 10 healthy and n = 18 Parkinson's disease lines). Kruskal-Wallis test, Dunn's multiple comparisons test: *p = 0.0067. Healthy: two-tailed paired t test, $^{\#}$p = 0.0194, df = 8. Parkinson's disease: Wilcoxon matched pairs signed rank test, $^{\#\#}$p = 0.0098, rs = 0.339. Data are expressed as mean ± the SD.

(C) Quantification of HSC70-positive puncta in neurites of TH-positive iDANs (mean average of 95 TH-positive cells assessed per line, n = 8–9 healthy and n = 16 Parkinson's disease lines). Mann-Whitney U test: *p = 0.0128, U = 26.5. Wilcoxon matched pairs signed rank test: $^{\#\#}$p = 0.0031, rs = 0.395. CT, control; H, healthy; PD, Parkinson's disease; ST, starved. Data are expressed as mean ± the SD.

basal rate of CMA in PD-iDANs (Figures 2A and 2B). Importantly, starvation induced a decrease in LAMP2a-positive cytoplasmic puncta in neurites only in H-iDANs, suggesting that PD-iDANs have an altered response to starvation, and that this alteration is specific to the DA subtype (Figures 2A and 2B). We next looked at HSC70 expression, the main chaperone responsible for the degradation of αSYN via CMA (Cuervo and Wong, 2014). Both parental aHDFs from healthy and PD donors showed a decrease in HSC70 expression in response to starvation (Figures S2H and S2I). While the number of HSC70-positive puncta in the neurites of starved H-iDANs increased (154.0% ± 117.2% of the non-starved condition), starvation-induced autophagy led to a decrease of HSC70-positive puncta in PD-iDANs (55.9% ± 28.1% of the non-starved condition) (Figure 2C). At baseline, an increase in the colocalization between HSC70 and αSYN was observed in iDANs from the PD group compared with healthy controls (Figure S2O). However, this was not accompanied by a decrease in αSYN in PD-iDANs following starvation (Figures S2P and S2Q). Taken together, these results suggest that there is both an alteration in baseline CMA as well as stress-induced autophagy that is specific to idiopathic PD-derived iDANs.

Altered macroautophagy response to stress-induced autophagy in iNs from PD patients

CMA preferentially degrades specific proteins, rather than organelles and other macromolecules (Salvador et al., 2000). However, while there is considerable crosstalk between CMA and macroautophagy, starvation predominantly induces macroautophagy, a process involving the formation of double-membraned autophagosomes that

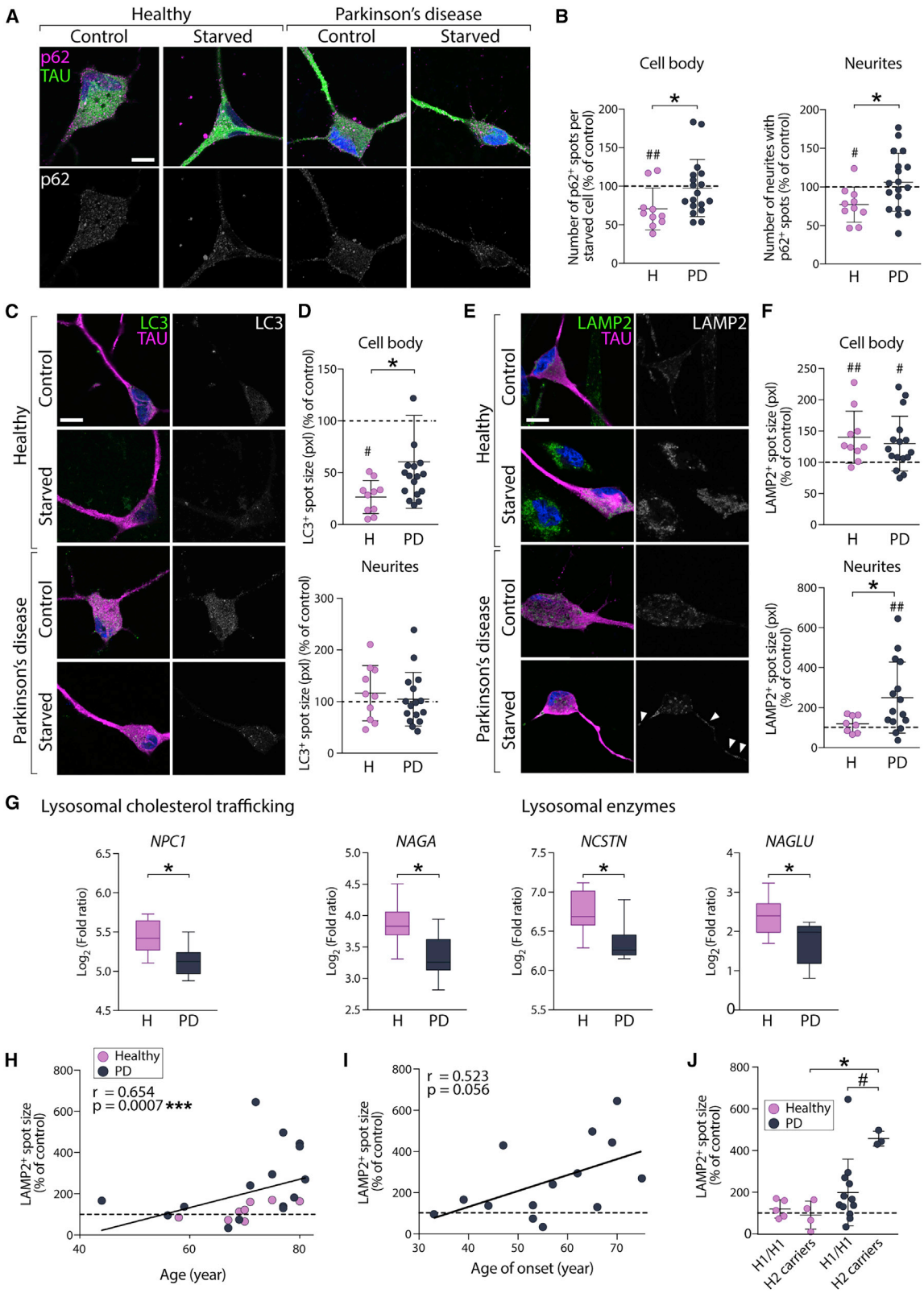

(legend on next page)

fuse with lysosomes, resulting in degradation of their contents. Given that we observed CMA alteration in PD-iDANs in response to starvation, we sought to further investigate whether there is an impairment in macroautophagy in PD-iNs. To validate the activation of macroautophagy upon starvation, we first looked at the cargo receptor p62, which decreases in the context of nutrient deprivation (Pircs et al., 2012). In the parental aHDFs, our starvation regimen induced a decrease in p62-positive cytoplasmic puncta in both healthy and PD donor-derived lines (Figures S3A and S3B). This decrease was also observed in H-iNs (70.6% ± 27.2% of the non-starved condition in the cell body and 77.1% ± 22.8% in neurites) (Figures 3A and 3B). However, once converted to neurons, the majority of PD lines failed to degrade p62 upon starvation, resulting in an accumulation of p62-positive puncta in PD-iNs compared with H-iNs, which was observed in all TAU-positive iNs, regardless of the neuronal subtype or neuronal compartment (97.5% ± 37.1% of the non-starved condition in the cell body and 106.0% ± 37.4% in neurites) (Figures 3A and 3B; see representative images of the puncta quantified in Figures S3G–S3I). We then assessed more specifically microtubule-associated protein 1 light chain 3 beta (LC3) to identify autophagic structures (Pircs et al., 2018). We found that starvation significantly reduced the size of LC3-positive cytoplasmic puncta in the cell bodies of H-iNs (26.5% ± 15.9% of the non-starved condition). However, LC3-positive cytoplasmic puncta in the cell body of PD-iNs were not significantly smaller after starvation (56.5% ± 44.2% of the non-starved condition). When comparing the level of size reduction of LC3-positive cytoplasmic puncta in the cell body after starvation, PD-iNs failed to reduce puncta size to the level that was seen in the H-iN group (Figures 3C and 3D), whereas no effect of starvation was observed in the neurites of H-iNs and PD-iNs (116.3% ± 53.6% of the non-starved condition for H-iNs, and 104.4% ± 51.8% for PD-iNs). Furthermore, this difference in macroautophagy between H-iNs and PD-iNs in the cell bodies was a cell-type-specific feature as it was not seen in the parental aHDFs (Figures S3C and S3D).

Once autophagosomes have enclosed their autophagy substrates, they can fuse with endosomes or lysosomes to form amphisomes and autolysosomes. We thus used LAMP2 (detecting all three isoforms: LAMP2a, LAMP2b, and LAMP2c) to visualize these structures. LAMP2-positive cytoplasmic puncta decreased upon starvation in the parental aHDFs of PD lines (Figures S3E and S3F). However, while an increase of the size of these structures upon starvation was similar in the cell bodies of both H- and PD-iNs (140.1% ± 41.6% of the non-starved condition for H-iNs and 130.06% ± 43.8% for PD-iNs), in the neurites, the size of LAMP2-positive puncta was unaffected by starvation in H-iNs (118.9% ± 42.3% of the non-starved condition), whereas they were significantly bigger in PD-iNs (251.8% ± 177.7% of the non-starved condition) (Figures 3E and 3F). Unlike the altered CMA

Figure 3. Accumulation of p62, LC3, and LAMP2 in PD-iNs upon starvation

(A) p62-positive dot expression in TAU-positive iNs. Scale bar, 10 μm.

(B) Quantification of p62-positive puncta in TAU-positive iNs (mean average of 577 TAU-positive cells assessed per line, n = 10 healthy and n = 18 Parkinson's disease lines). Cell body: Mann-Whitney test, *p = 0.0400; healthy, two-tailed paired t test, $^{\#\#}$p = 0.0056, df = 9. Neurite: unpaired t test, *p = 0.0357, df = 26, healthy, two-tailed paired t test, $^{\#}$p = 0.0128, df = 9. Data were normalized as percentage of control condition (not starved) and are expressed as mean ± the SD.

(C) LC3-positive dot expression in TAU-positive iNs. Scale bar, 10 μm.

(D) Quantification of LC3-positive puncta in TAU-positive iNs (mean average of 479 TAU-positive cells assessed per line, n = 10 healthy and n = 18 Parkinson's disease lines). Cell body: two-tailed Mann-Whitney U test, *p = 0.0311, U = 51; healthy, two-tailed paired t test, $^{\#\#}$p = 0.0051, df = 9. Data were normalized as percentage of control condition (not starved) and are expressed as mean ± the SD.

(E) LAMP2-positive dot expression in TAU-positive iNs. Scale bar, 10 μm.

(F) Quantification of LAMP2-positive puncta in TAU-positive iNs (mean average of 202 TAU-positive cells assessed per line, n = 10 healthy and n = 17 Parkinson's disease lines). Cell body: healthy, two-tailed paired t test, $^{\#\#}$p = 0.0078, df = 8; Parkinson's disease, $^{\#}$p = 0.0295, df = 13. Neurites: two-tailed unpaired t test with Welch's correction, *p = 0.0136, U = 24; *p = 0.0125, df = 18.23. Parkinson's disease: two-tailed paired t test, $^{\#\#}$p = 0.0042, df = 16.75. Data were normalized as percentage of control condition (not starved) and are expressed as mean ± the SD.

(G) Boxplots of $\log_2$ fold changes in expression of genes associated with lysosomal functions (adjusted p value <0.09, n = 10 healthy and n = 10 Parkinson's disease lines). Data are expressed as mean ± the SD.

(H) Accumulation of LAMP2-positive puncta upon stress-induced autophagy is associated with the age of the donor (n = 23 lines). Spearman's rank correlation: ***p = 0.0007; 95% confidence interval, 0.3199–0.8437.

(I) Association between accumulation of LAMP2-positive puncta upon stress-induced autophagy and the age of onset of Parkinson's disease (n = 14 Parkinson's disease lines). Spearman's rank correlation: p = 0.056; 95% confidence interval, 0.01127–0.8263.

(J) More pronounced accumulation of LAMP2-positive puncta upon stress in *MAPT H2* carrier Parkinson's disease patients. Kruskal-Wallis test, Dunn's multiple comparisons test: *p = 0.0265. Two-tailed Mann-Whitney U test: $^{\#}$p = 0.0250, U = 3. Data are expressed as mean ± the SD. CT, control; H, healthy; PD, Parkinson's disease; ST, starved.

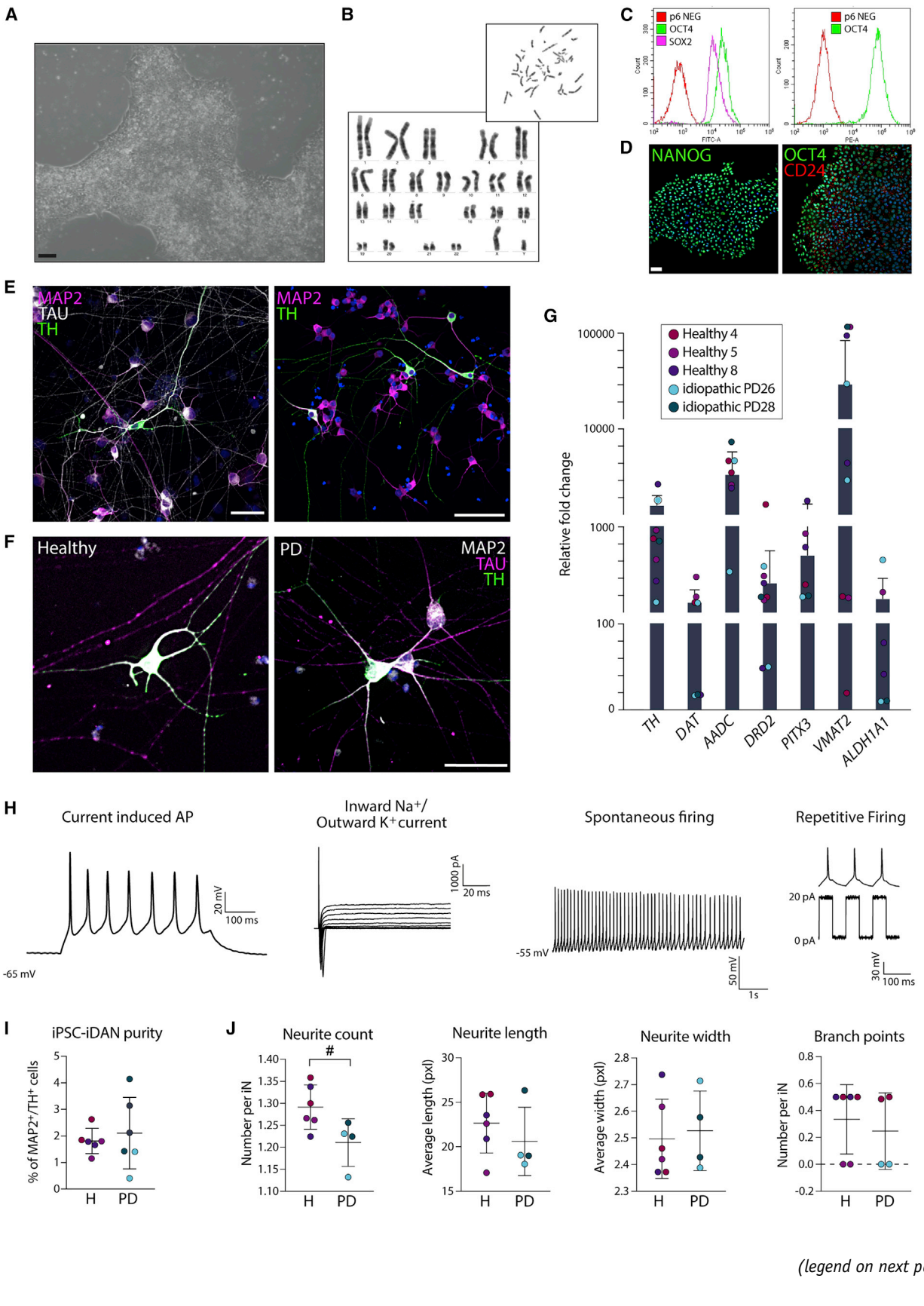

(legend on next page)

response (Figures 2A–2C), these phenotypes were present in all iNs and not just DA neurons (Figure S4). Blocking the autophagic flux using bafilomycin A1 led to an accumulation of LC3-positive puncta in the cell body of H-iNs. However, this accumulation of autophagosomes was absent in PD-iNs (Figures S6C–S6E), indicating possible impairment at early steps of the autophagic process, as also supported by a downregulation of early autophagy-related genes in PD-iNs (Figure S6F).

To assess whether this altered autophagy response could be due to basal changes in the transcriptome of PD-iNs, we performed RNA sequencing (RNA-seq) analysis on the iNs and the parental aHDFs. This analysis confirmed there was a major change in gene expression profile as aHDFs were reprogrammed toward a neuronal phenotype (Figure S5). Moreover, gene set enrichment analysis (GSEA) using Kyoto Encyclopedia of Genes and Genomes (KEGG) pathways identified genes in the lysosome pathway (hsa014142) to be significantly enriched (adjusted p value = 0.026) (Figure S6A). When analyzing specifically the lysosomal genes, we found that the lysosomal cholesterol trafficking gene *NPC1* involved in the inherited metabolic disease Niemann-Pick, type C (Park et al., 2003) as well as three other lysosomal enzymes (*NAGA*, *NCSTN*, *NAGLU*) were downregulated in PD-iNs compared to H-iNs (Figure 3G), supporting the data suggesting that there are alterations in lysosomal functions at baseline and in line with observations that these inherited disorders can lead to parkinsonian states clinically and pathologically (Winder-Rhodes et al., 2012). Importantly, when analyzing expression of these genes between the healthy controls and PD patients in parental aHDFs, they were not differentially expressed (Figure S6B).

Age-related correlation in disease-associated impairments and accumulation of phosphorylated αSYN

Recent reports have shown that age-associated properties of the human donors are maintained in iNs but not in iPSC-derived neurons (Capano et al., 2022; Huh et al., 2016; Kim et al., 2018; Mertens et al., 2015, 2021; Tang et al., 2017). We therefore assessed whether the accumulation of lysosomal structures in H- and PD-iNs was associated with the age of the donor. We found a positive correlation between the age and the accumulation of lysosomes in neurites (Figure 3H), and a trend toward a positive correlation of this accumulation with age of onset at diagnosis (Figure 3I). This was more pronounced in lines derived from patients carrying the H2 haplotype of *MAPT*, which has previously been associated with a more rapid progression and cognitive decline in PD and other neurodegenerative disorders (Figure 3J) (Valenca et al., 2016; Vuono et al., 2015).

To further study donor age and how this affects disease-related pathology, we next established iPSC lines from the aHDFs of two patients (with a high amount of pathology as quantified in the iNs derived from same patient's aHDFs) and three controls (see Table 1). The cells were reprogrammed into iPSCs using the StemRNA 3rd Generation Reprogramming Kit (Figure 4A). Quality control analysis confirmed that the iPSCs retained a normal karyotype (Figure 4B), and expression of pluripotency markers was confirmed using immunocytochemistry and flow analysis (Figures 4C and 4D). We then confirmed that the same protocol developed for the fibroblast-to-iDAN conversion (Figure 1A) also converted iPSCs to functional iDANs (Figures 4E and 4F). iPSC-iDANs expressed high levels of DA-related genes (Figure 4G) and were functionally mature (Figure 4H). Similarly to fibroblast-derived iDANs, there was no difference in neuronal purity, although a slightly lower neurite count was observed in iPSC-derived iDANs from PD patients (Figures 4I and 4J).

Next, we used RNA-seq from iNs derived from aHDFs (Fib-iNs) and iNs derived from iPSCs (iPSC-iNs) from the same individuals to assess age-related aspects in the resulting neurons (Figure 5A). First, GSEA was performed to determine if any molecular features relating to cellular

Figure 4. Generation of iDANs from iPSCs of healthy donors and idiopathic PD patients

(A) Brightfield images of fibroblasts reprogrammed to iPSCs using a StemRNA 3rd Generation Reprogramming Kit. Scale bar, 100 μm.
(B) Cells retained a normal karyotype.
(C) FACS quantification of stem cell markers OCT4, SOX2, and CD24.
(D) Immunofluorescence staining showing that cells express stem cell markers NANOG, OCT4, and CD24. Scale bar, 50 μm.
(E) MAP2-positive, TAU-positive, and TH-positive iPSC-iDANs. Cells are counterstained with DAPI (in blue). Scale bars, 100 μm.
(F) Representative images of MAP2-positive, TAU-positive, and TH-positive iPSC-iDANs derived from healthy donors and PD patients. Cells are counterstained with DAPI (in blue). Scale bars, 25 μm.
(G) Quantitative RT-PCR gene expression quantification of DA genes relative to parental iPSC levels (nine clones from five lines). Refer to Table 1 for information on each donor from which the iPSC cell lines were derived. Data are expressed as mean ± the SD.
(H) Patch clamp recordings of iDANs reprogrammed from RC17 embryonic stem cells at day 35 (n = 8 neurons).
(I) Quantification of double-MAP2-positive and TH-positive cells (from two clones; six well replicates). Data are expressed as mean ± the SD.
(J) Quantification of neurite profile in TAU-positive H-iNs and PD-iNs derived from iPSCs (from two clones; six well replicates). Data are expressed as mean ± the SD.

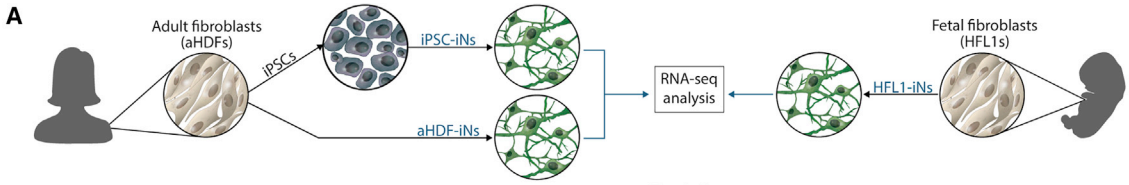

B

Description	Set size	Enrichment Score	NES	*p* value	*p*-adjust
GO_MULTICELLULAR_ORGANISM_AGING	28	-0.627	-1.872	0.003	0.015
GO_AGING	265	0.296	1.120	0.217	0.460
GO_NEGATIVE_REGULATION_OF_CELL_AGING	21	-0.432	-1.201	0.230	0.460
GO_REGULATION_OF_CELL_AGING	42	-0.320	-1.015	0.425	0.594
GO_POSITIVE_REGULATION_OF_CELL_AGING	12	-0.372	-0.887	0.581	0.594
GO_CELL_AGING	96	-0.249	-0.935	0.594	0.594

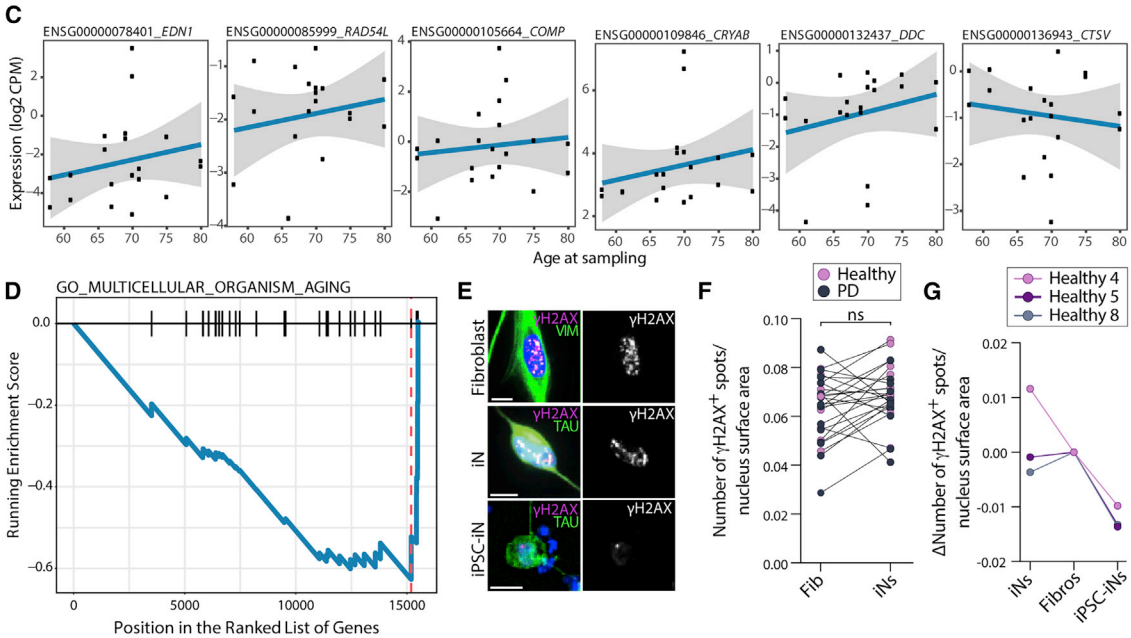

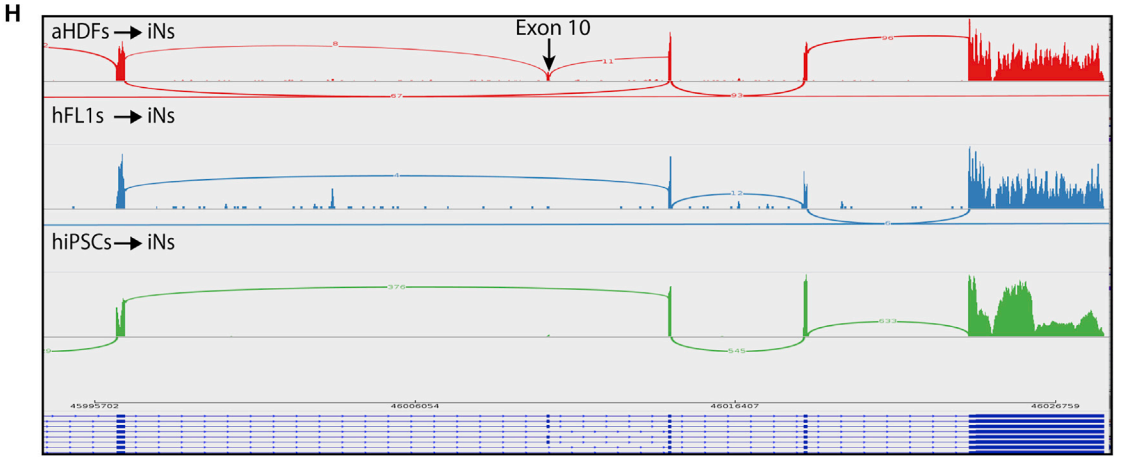

(legend on next page)

aging were associated with the donor age in Fib-iNs. Genes were ranked based on their association (using the Pearson correlation coefficient) with age at sampling and six gene sets related to aging were extracted from the Gene Ontology database. Despite the limited age span of the donors included in this analysis (58–80 years old), we observed a positive correlation between donor age with expression of an age-related gene signature (normalized enrichment score 1.4, adjusted p value = 0.015) in Fib-iNs (adjusted p value = 0.4; Figures 5B–5D). To complement the GSEA data, we also looked at DNA damage, another independent marker of cellular aging, using γH2AX. This analysis comparing the number of γH2AX spots in the nucleus of parental aHDFs with reprogrammed iNs showed a maintenance of the number of γH2AX spots after 27 days of conversion, which was not the case following reprograming of these same cell lines to iPSC-iNs, indicating a rejuvenation of the cells during reprograming to pluripotency (Figures 5E–5G). Next, we looked at the presence of the isoforms of TAU expressed in adult mature neurons. There are three TAU isoforms with three repeats (3R) and three with four repeats (4R). Neurons generated from iPSCs very strongly express the 3R isoforms but do not express the 4Rs at the protein level, even after 1 year of *in vitro* maturation (Sposito et al., 2015), reflecting the expression of only the 3Rs of TAU at the human embryonic stage. This analysis showed that exon 10 (giving rise to 4R isoforms) is only expressed in iNs from aHDFs (in ∼40% of transcripts), and not in iNs derived from fetal fibroblasts or from iPSCs (Figure 5H). Moreover, the 3R/4R ratio for aHDFs was 23%, whereas it was <1% for hFL1s. Taken together, this analysis suggests that donor age is at least partially maintained during iN conversion but erased during iPSC reprogramming, similar to other reports (Capano et al., 2022; Mertens et al., 2015; Tang et al., 2017).

Phosphorylated αSYN is a hallmark of PD pathology and this has been recapitulated in some iPSC-based cellular models of genetic forms of PD (Kouroupi et al., 2017; Lin et al., 2016) but not idiopathic PD. We therefore sought to investigate whether alterations in stress-induced autophagy observed in Fib-iNs from idiopathic PD patients could lead to changes in the levels of phosphorylated αSYN at the serine 129 site (pSer129 αSYN). We found that while a concurrent activation of macroautophagy by starvation and a blockage of the flux with bafilomycin A1 did not induce significant changes in pSer129 αSYN in H-iNs (83.1% ± 53.9% of the starved condition), it did lead to an increase in the number of PD-iNs with pSer129 αSYN-positive cytoplasmic dots (126.5% ± 54.0% of the starved condition) (Figures 6A and 6B). This increase was also observed when looking specifically at PD-iDANs (128.1% ± 21.4% of the starved condition), compared with H-iDANs, which again did not show any changes in pSer129 αSYN upon bafilomycin A1 treatment (98.2% ± 16.0% of the starved condition) (Figures 6D and 6E). Positive correlation between the accumulation of 81A-positive puncta in two independent experiments evaluating the pSer129 αSYN spot expression in iNs and in iDANs showed that the same cell lines are prone to pSer129 αSYN accumulation independently of the neuronal subtype, and demonstrates the reproducibility of these experiments (Figure S6G). Interestingly, for some of the results including pSer129 αSYN, p62, and LAMP2 accumulation, subanalyses allowed a stratification of the PD patient population based on their age and age at onset (Figures S3J and S6I). Finally, to assess whether elevated basal levels of total αSYN could explain the elevated levels of pSer129 αSYN observed in lines starved and treated with bafilomycin A1, we plotted the measure of the total αSYN fluorescence intensity against the pSer129 αSYN expression

Figure 5. Assessment of cellular aging

(A) Overview of RNA-seq experiment.

(B) Gene set enrichment analysis (GSEA) showing enrichment scores of pathways related to cell aging.

(C) Top genes showing a clear increase in expression with age were extracted from the Gene Ontology database and queried against using GSEA (as implemented in the clusterProfiler R package). Five out of six of these gene sets showed negative enrichment scores, indicating association of aging with donor age in this dataset.

(D) Multicellular organism aging showing a significant enrichment score.

(E) Representative image of γH2AX expression in TAU-positive iNs, parental fibroblasts and iPSC-iNs, all from line #18 (87 years old). Scale bar, 10 μm.

(F) Quantification of γH2AX-positive puncta in TAU-positive iNs and parental fibroblasts (mean average of 1,327 fibroblasts and 1,210 TAU-positive cells assessed per line, n = 26 lines). Two-tailed paired t test: p = 0.071, df = 25.

(G) Quantification of γH2AX-positive puncta in TAU-positive iNs, parental fibroblasts and iPSC-iNs (mean average of n = 329 fibroblasts, n = 833 TAU-positive iNs, and n = 24 iPSC-iNs assessed per line, n = 3 lines). Refer to Table 1 for the information of each donor from which the iPSC cell lines were derived.

(H) Sashimi plots visualizing splice junctions and genomic coordinates from merged bam files from adult Fib-iNs (red) and fetal Fib-iNs (blue) indicating that expression of exon 10 (4R isoforms) is only present in iNs from adult fibroblasts. Height of bars indicates expression level and the number on the lines gives number of reads spanning that splice junction. ns, not significant; Vim, vimentin.

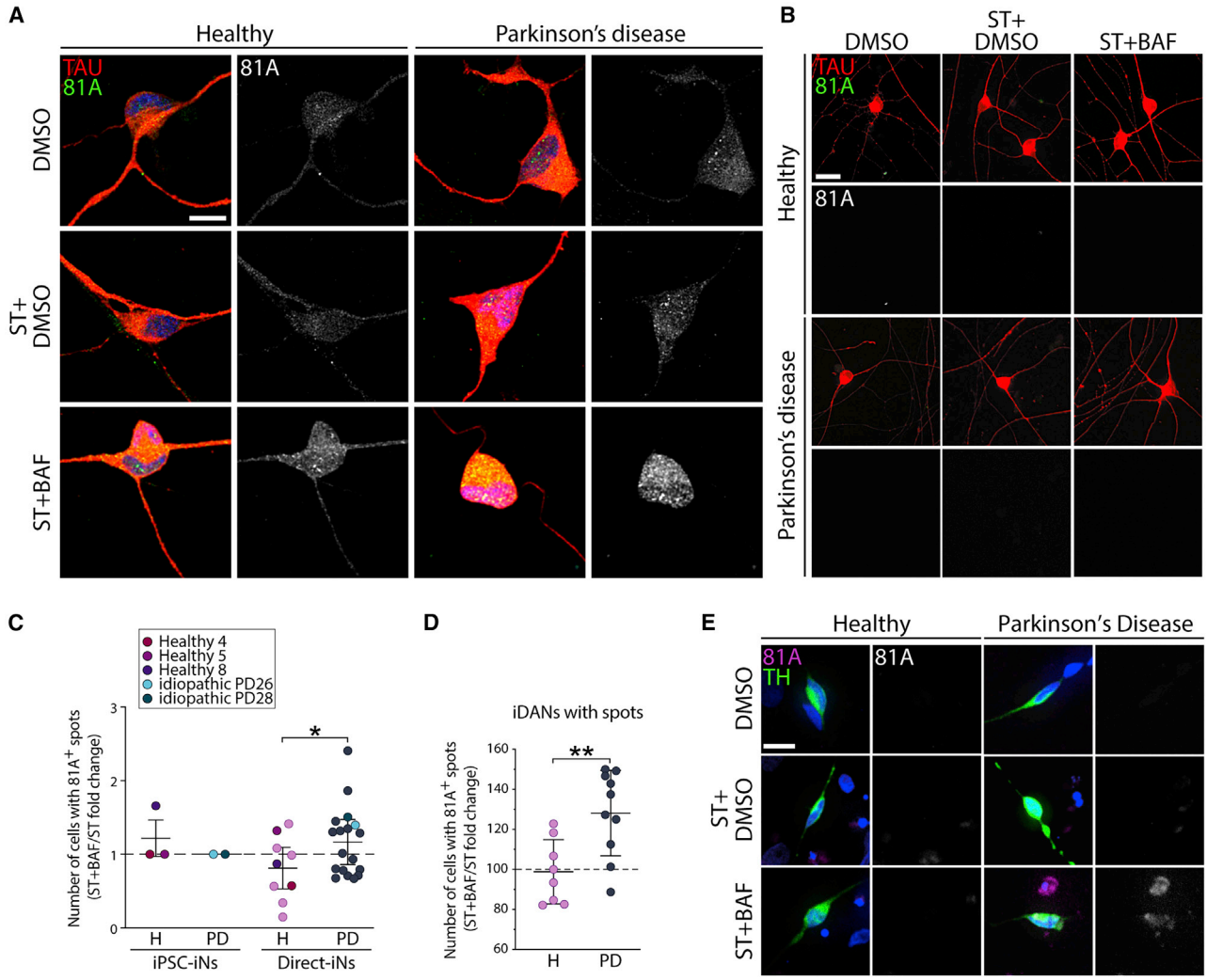

Figure 6. Autophagy impairments lead to an accumulation of phosphorylated αSYN in PD-iNs and PD-iDANs

(A) Confocal images of 81A-positive dot expression in TAU-positive iNs directly reprogrammed from fibroblasts. Scale bar, 10 μm.

(B) Fluorescent images of 81A-positive dot expression in TAU-positive iNs reprogrammed from iPSCs. Scale bar, 25 μm.

(C) Quantification of TAU-positive iNs with 81A-positive (pSer129 αSYN) puncta in the cell body (iPSCs-iNs: mean average of 180 TAU-positive cells assessed per line, n = 3 healthy and n = 2 PD lines. Direct-iNs: mean average of 1,461 TAU-positive cells assessed per line, n = 9 healthy and n = 18 PD lines). Two-tailed unpaired t test: *p = 0.0329, df = 25. Refer to Table 1 for the information of each donor from which the iPSC cell lines were derived. Data are expressed as mean ± the SD.

(D) Quantification of TAU-positive/TH-positive iDANs with 81A-positive puncta in the cell body (mean average of 28 TAU-positive/TH-positive cells assessed per line, n = 8 healthy and n = 10 PD lines). Two-tailed unpaired t test: **p = 0.0054, df = 16. Data are expressed as mean ± the SD.

(E) 81A-positive dot expression (in magenta) in TH-positive iDANs (in green) directly reprogrammed from fibroblasts. Scale bar, 25 μm.

BAF, bafilomycin A1; H: healthy; PD, Parkinson's disease; ST, starved.

measured in iDANs. There was no correlation between basal total αSYN levels and the bafilomycin A1-induced accumulation of pSer129 αSYN in iDANs (Figure S6H), suggesting that the increase seen in the PD group is not due to higher basal αSYN expression (Figures S2L–S2N). When assessing iN reprogrammed from iPSCs established from the two PD lines showing the most pSer129 αSYN accumulation in fibroblast-derived iNs and iDANs as well as three control lines (Table 1), we could not detect any pSer129 αSYN puncta in the resulting iPSC-iNs in these lines (Figures 6B and 6C), supporting that the maintenance of age in iNs is important for modeling the αSYN pathophysiology of idiopathic PD.

DISCUSSION

We report on an improved cellular model of idiopathic PD using a *REST* knockdown approach to enable neuronal gene transcription in aHDFs (Drouin-Ouellet et al., 2017), combined with an optimal combination of DA fate determinants (*Lmx1a*, *Lmx1b*, *Foxa2*, *Otx2*, *Nr4a2*). This new direct reprogramming approach increased the efficiency, subtype identity, and functional maturation of iDANs during direct conversion, making it possible to perform studies at a scale suitable for disease modeling, drug screening, and other biomedical applications. The model is much less labor intensive and cost-effective than iPSC-modeling, which allowed us to compare iNs from 18 different idiopathic PD patients that were all processed at the same time. Moreover, it maintains the donor's age and reflect pathological changes after only 25 days.

We observed alterations in stress-induced autophagy across the different patient-derived iNs compared with healthy donor lines. We found that blocking the autophagic flux through the inhibition of the fusion of autophagosomes with lysosomes resulted in accumulation of pSer129 αSYN in PD-iNs and PD-iDANs. These impairments of autophagy-lysosomal function may reflect the effect of the important presence of variants of genes related to lysosomal storage disorders in the PD patient population. Indeed, a recent study reported that more than half of the cases in a PD patient cohort harbored one or more putative damaging variants among the lysosomal storage disorders genes, suggesting the possibility that these variants may interact in a multi-hit, combinatorial manner to degrade lysosomal function, causing the accumulation of αSYN and increasing susceptibility to PD (Robak et al., 2017). Future studies using lines derived from patients with strong genetic forms of PD will also help our understanding of the phenotypes found in the idiopathic PD lines and how they relate to different pathways disrupted in familial PD.

Disease-associated impairment could not be detected in the parental aHDFs, nor in the same cells when they were first reprogrammed to pluripotency and then converted to DA neurons. This shows that direct conversion of aHDFs, where age-related aspects of the donor are maintained, provides a faithful cell-based model of idiopathic PD. Importantly, our cellular model showed that iNs from different patients are not impaired to the same degree. We found that the degree of impairment relates, at least to some extent, to the age of the donor, the age at PD onset, and the *MAPT* haplotype. This effect of age and genetic variance on disease pathology has not been recapitulated in cellular models before, and suggests that direct conversion to iDANs could be used for differential diagnostics, drug screening, and disease modeling of late-onset neurogenerative diseases while also capturing the heterogeneity of disease that is apparent clinically.

In this respect, our results demonstrate the utility of establishing models of neurodegenerative disorders with cells that resemble the subtype and functionality of the affected neurons in individual patients as closely as possible. For example, we could not detect any autophagy-related impairment in the aHDFs prior to conversion, clearly demonstrating that the reprogramming to neurons is essential to reveal disease-related phenotypes. Also, specific CMA impairments were detected only in iNs with a DA phenotype.

While it is hard to draw exact parallels between stem-cell derived neurons formed via developmental principles and directly converted neurons, both systems have their own merits. Of importance here is that the aging signature of the donor cell is maintained during direct conversion when postmitotic neurons are formed without a proliferative intermediate. Our data support the maintenance of donor age, which uniquely allows for modeling age-related aspects of PD. Future studies using this cellular model will thus contribute to a deeper understanding of the age-associated pathology of PD along with the cellular basis of disease subtypes and variable progression and, by so doing, allow us to better develop and assess novel therapeutic interventions.

EXPERIMENTAL PROCEDURES

Cell lines

aHDFs were obtained from the Parkinson's Disease Research Clinic at the John van Geest Centre for Brain Repair (Cambridge, UK) and used under full local ethical approvals: REC 09/H0311/88 (University of Cambridge) and CERSES-18-004-D (University of Montreal) (Table 1). The subjects' consent was obtained according to the declaration of Helsinki. Cell lines used in this study will be made available to others subject to appropriate ethical approval and an MTA from the requestor. For biopsy sampling information see Drouin-Ouellet et al. (2017).

Neural reprogramming

For direct neural reprogramming, aHDFs were plated at a density of 26,300 cells/cm^2 in 24-well plates (Nunc) according to a previously published protocol (Shrigley et al., 2018). Prior to plating, the wells were coated overnight with either 0.1% gelatin (Sigma), or a combination of polyornithine (15 μg/mL), fibronectin (0.5 ng/μL), and laminin (5 μg/mL). To assess the reprogramming efficiency of each line, all 28 lines were reprogrammed at the same time with the same virus mixture, and this was repeated three times using different batches of virus for each of the eight lentiviral vectors required for the iDAN reprogramming.

Starvation and bafilomycin A1 treatment

On day 28 following viral transduction, iNs were starved for 4 h by replacing the culture medium with HBSS and Ca^{2+}/Mg^{2+} and

compared with the condition without starvation, where cells were left in their original culture medium. The duration of starvation treatment was chosen based on a starvation curve performed on the iNs (0, 2, and 4 h), which showed clear increases in p62 and LC3 expression by WB in the absence of neuronal cell death (Figures S2D and S2E). For the experiment with bafilomycin A1, cells were starved in HBSS Ca^{2+}/Mg^{2+} containing bafilomycin A1 (100 nM; Sigma Aldrich) for 2 h and compared with cells incubated in HBSS Ca^{2+}/Mg^{2+} containing dimethyl sulfoxide (DMSO; vehicle). This regimen was chosen based on the increase of LC3-II and the LC3-II/LC3-I ratio as assessed by WB. At the end of the incubation period, cells were fixed in 4% paraformaldehyde.

High-content screening quantifications

The total number of DAPI-positive, TAU-positive, and TH-positive cells per well, as well as the average fluorescence intensity for αSYN, was quantified using the Cellomics Array Scan (Array Scan VTI, Thermo Fisher). Average dot number and size were measured in those neurons in which the cytoplasm and neurites were defined by TAU or TH staining. Puncta of p62, LC3, LAMP2, LAMP2a, HSC70, αSYN, and 81A were detected (using a spot-detection program) and measured in each case. Images with cells with extreme values were manually verified to make sure that poor focus was not underlying these results. The primary antibodies used are listed in Table S1. Cell images in Figures 2, 3A, 3C, 3E, 6A, 6B, and 6E are representatives images acquired by confocal microscopy (Zeiss LSM800) at 63×.

Statistical analysis

All data are expressed as mean ± the SD. Whenever the analysis is performed with one cell line, three to four well replicates were used. In case of experiments using multiple cell lines, we used a minimum of n = 6 to account for inter-individual variation. A Shapiro-Wilk normality test was used to assess the normality of the distribution. When a normal distribution could not be assumed, a non-parametric test was performed. Groups were compared using a one-way ANOVA with a Bonferroni post hoc or a Kruskal-Wallis test with a Dunn's multiple comparisons tests. To determine whether there was a significant difference between two sets of observations repeated on the same lines, a paired sample t test was also performed. In cases of only two groups, they were compared using a Student's t test. An F test was used to compare variance and, in cases of unequal variance, a Welch's correction test was then performed. Statistical analyses were conducted using the GraphPad Prism 7.0. An alpha level of $p < 0.05$ was set for significance.

See supplemental experimental procedures for further details.

Data and code availability

The accession number for the RNA-seq dataset reported in this paper is GEO: GSE125239.

SUPPLEMENTAL INFORMATION

Supplemental information can be found online at https://doi.org/10.1016/j.stemcr.2022.08.010.

AUTHOR CONTRIBUTIONS

J.D.-O., K.P., J.J., R.A.B., and M. Parmar designed the research. J.D.-O., E.M.L., F.N., K.P., J.B., F.P., M.B., S.S., M. Pereira, A.B., M.K., R.V., T.B.S., and K.P. performed the research. D.R.O., A.F., and R.A.B. contributed new reagents/analytic tools. J.D.-O., E.M.L., F.N., K.P., J.B., F.P., M.B., S.S., P.S., Y.S., R.V., and K.P. analyzed data. J.D.-O. and M. Parmar wrote the first draft of the paper.

ACKNOWLEDGMENTS

We thank Marie Persson Vejgården, Sol Da Rocha Baez, Ulla Jarl (Lund University), as well as Dr. Anna Hammarberg at the MultiPark Cellomics platform at Lund University and Simon-Pierre Gravel (U. Montreal) for their valuable help with high content imaging. This research has received funding from the NYSCF, the ERC FP/2007–2013 NeuroStemcellRepair (no. 602278 and ERC no. 771427), the Swedish Research Council (2016-00873), Parkinsonfonden, Hjärnfonden (FO2019-0301), Olle Engkvist Foundation 203-0006 (J.J.), the Strategic Research Areas at Lund University MultiPark and StemTherapy, the Cure Parkinson's Trust in the UK (RAB), and Parkinson Canada (2018-00236) (J.D.-O.). This research was also supported by the Canada Research Chair Program and the NIHR Cambridge Biomedical Research Centre (BRC-1215-20014). The views expressed are those of the authors and not necessarily those of the NIHR or the Department of Health and Social Care. This research was funded in part by the Wellcome Trust 203151/Z/16/Z. For the purpose of open access, the author has applied a CC BY public copyright license to any author-accepted manuscript version arising from this submission. R.A.B. was a NIHR Senior Investigator. M. Parmar is an NYSCF - Robertson Investigator. J.D.-O. is a Canada Research Chair and received support from FRQS in partnership with Parkinson Québec (#268980) and the Canada Foundation for Innovation (#38354). M.B. and S.S. were funded by the European Union Horizon 2020 Programme (H2020-MSCA-ITN-2015; no. 676408). E.M.L. is supported by an FRQS Graduate Scholarship in partnership with Parkinson Canada.

CONFLICTS OF INTERESTS

M. Parmar, J.J., and J.D.-O. are co-inventors of the patent application PCT/EP2018/062261 owned by New York Stem Cell Foundation. M. Parmar is the owner of Parmar Cells AB.

Received: August 24, 2021
Revised: August 25, 2022
Accepted: August 25, 2022
Published: September 22, 2022

REFERENCES

Ambasudhan, R., Talantova, M., Coleman, R., Yuan, X., Zhu, S., Lipton, S.A., and Ding, S. (2011). Direct reprogramming of adult human fibroblasts to functional neurons under defined conditions. Cell Stem Cell *9*, 113–118.

Brazdis, R.M., Alecu, J.E., Marsch, D., Dahms, A., Simmnacher, K., Lörentz, S., Brendler, A., Schneider, Y., Marxreiter, F., Roybon, L., et al. (2020). Demonstration of brain region-specific neuronal

vulnerability in human iPSC-based model of familial Parkinson's disease. Hum. Mol. Genet. *29*, 1180–1191.

Caiazzo, M., Dell'Anno, M.T., Dvoretskova, E., Lazarevic, D., Taverna, S., Leo, D., Sotnikova, T.D., Menegon, A., Roncaglia, P., Colciago, G., et al. (2011). Direct generation of functional dopaminergic neurons from mouse and human fibroblasts. Nature *476*, 224–227.

Capano, L.S., Sato, C., Ficulle, E., Yu, A., Horie, K., Kwon, J.S., Burbach, K.F., Barthélemy, N.R., Fox, S.G., Karch, C.M., et al. (2022). Recapitulation of endogenous 4R tau expression and formation of insoluble tau in directly reprogrammed human neurons. Cell Stem Cell *29*, 918–932.e8.

Cuervo, A.M., Stefanis, L., Fredenburg, R., Lansbury, P.T., and Sulzer, D. (2004). Impaired degradation of mutant alpha-synuclein by chaperone-mediated autophagy. Science *305*, 1292–1295.

Cuervo, A.M., and Wong, E. (2014). Chaperone-mediated autophagy: roles in disease and aging. Cell Res. *24*, 92–104.

Drouin-Ouellet, J., Lau, S., Brattås, P.L., Rylander Ottosson, D., Pircs, K., Grassi, D.A., Collins, L.M., Vuono, R., Andersson Sjöland, A., Westergren-Thorsson, G., et al. (2017). REST suppression mediates neural conversion of adult human fibroblasts via microRNA-dependent and -independent pathways. EMBO Mol. Med. *9*, 1117–1131.

Huh, C.J., Zhang, B., Victor, M.B., Dahiya, S., Batista, L.F., Horvath, S., and Yoo, A.S. (2016). Maintenance of age in human neurons generated by microRNA-based neuronal conversion of fibroblasts. Elife 5, e18648.

Jiang, H., Xu, Z., Zhong, P., Ren, Y., Liang, G., Schilling, H.A., Hu, Z., Zhang, Y., Wang, X., Chen, S., et al. (2015). Cell cycle and p53 gate the direct conversion of human fibroblasts to dopaminergic neurons. Nat. Commun. *6*, 10100.

Kim, Y., Zheng, X., Ansari, Z., Bunnell, M.C., Herdy, J.R., Traxler, L., Lee, H., Paquola, A.C.M., Blithikioti, C., Ku, M., et al. (2018). Mitochondrial aging defects emerge in directly reprogrammed human neurons due to their metabolic profile. Cell Rep. *23*, 2550–2558.

Kirkeby, A., Nolbrant, S., Tiklova, K., Heuer, A., Kee, N., Cardoso, T., Ottosson, D.R., Lelos, M.J., Rifes, P., Dunnett, S.B., et al. (2017). Predictive markers guide differentiation to improve graft outcome in clinical translation of hESC-based therapy for Parkinson's disease. Cell Stem Cell *20*, 135–148.

Klionsky, D.J., Abdelmohsen, K., Abe, A., Abedin, M.J., Abeliovich, H., Arozena, A.A., Adachi, H., Adams, C.M., Adams, P.D., Adeli, K., et al. (2016). Guidelines for the use and interpretation of assays for monitoring autophagy (3rd edition). Autophagy *12*, 1–222.

Kouroupi, G., Taoufik, E., Vlachos, I.S., Tsioras, K., Antoniou, N., Papastefanaki, F., Chroni-Tzartou, D., Wrasidlo, W., Bohl, D., Stellas, D., et al. (2017). Defective synaptic connectivity and axonal neuropathology in a human iPSC-based model of familial Parkinson's disease. Proc. Natl. Acad. Sci. USA *114*, E3679–E3688.

Lang, C., Campbell, K.R., Ryan, B.J., Carling, P., Attar, M., Vowles, J., Perestenko, O.V., Bowden, R., Baig, F., Kasten, M., et al. (2019). Single-cell sequencing of iPSC-dopamine neurons reconstructs disease progression and identifies HDAC4 as a regulator of Parkinson cell phenotypes. Cell Stem Cell *24*, 93–106.e6.

Lapasset, L., Milhavet, O., Prieur, A., Besnard, E., Babled, A., Aït-Hamou, N., Leschik, J., Pellestor, F., Ramirez, J.M., De Vos, J., et al. (2011). Rejuvenating senescent and centenarian human cells by reprogramming through the pluripotent state. Genes Dev. *25*, 2248–2253.

Li, H., Jiang, H., Yin, X., Bard, J.E., Zhang, B., and Feng, J. (2019). Attenuation of PRRX2 and HEY2 enables efficient conversion of adult human skin fibroblasts to neurons. Biochem. Biophys. Res. Commun. *516*, 765–769.

Lin, L., Göke, J., Cukuroglu, E., Dranias, M.R., VanDongen, A.M.J., and Stanton, L.W. (2016). Molecular features underlying neurodegeneration identified through in vitro modeling of genetically diverse Parkinson's disease patients. Cell Rep. *15*, 2411–2426.

Luo, S.X., and Huang, E.J. (2016). Dopaminergic neurons and brain reward pathways: from neurogenesis to circuit assembly. Am. J. Pathol. *186*, 478–488.

Mertens, J., Herdy, J.R., Traxler, L., Schafer, S.T., Schlachetzki, J.C.M., Böhnke, L., Reid, D.A., Lee, H., Zangwill, D., Fernandes, D.P., et al. (2021). Age-dependent instability of mature neuronal fate in induced neurons from Alzheimer's patients. Cell Stem Cell *28*, 1533–1548.e6.

Mertens, J., Paquola, A.C.M., Ku, M., Hatch, E., Böhnke, L., Ladjevardi, S., McGrath, S., Campbell, B., Lee, H., Herdy, J.R., et al. (2015). Directly reprogrammed human neurons retain aging-associated transcriptomic signatures and reveal age-related nucleocytoplasmic defects. Cell Stem Cell *17*, 705–718.

Metzakopian, E., Bouhali, K., Alvarez-Saavedra, M., Whitsett, J.A., Picketts, D.J., and Ang, S.L. (2015). Genome-wide characterisation of Foxa1 binding sites reveals several mechanisms for regulating neuronal differentiation in midbrain dopamine cells. Development *142*, 1315–1324.

Miller, J.D., Ganat, Y.M., Kishinevsky, S., Bowman, R.L., Liu, B., Tu, E.Y., Mandal, P.K., Vera, E., Shim, J.w., Kriks, S., et al. (2013). Human iPSC-based modeling of late-onset disease via progerin-induced aging. Cell Stem Cell *13*, 691–705.

Nelander, J., Grealish, S., and Parmar, M. (2013). Human foetal brain tissue as quality control when developing stem cells towards cell replacement therapy for neurological diseases. Neuroreport *24*, 1025–1030.

Park, W.D., O'Brien, J.F., Lundquist, P.A., Kraft, D.L., Vockley, C.W., Karnes, P.S., Patterson, M.C., and Snow, K. (2003). Identification of 58 novel mutations in Niemann-Pick disease type C: correlation with biochemical phenotype and importance of PTC1-like domains in NPC1. Hum. Mutat. *22*, 313–325.

Pereira, M., Pfisterer, U., Rylander, D., Torper, O., Lau, S., Lundblad, M., Grealish, S., and Parmar, M. (2014). Highly efficient generation of induced neurons from human fibroblasts that survive transplantation into the adult rat brain. Sci. Rep. *4*, 6330.

Pfisterer, U., Kirkeby, A., Torper, O., Wood, J., Nelander, J., Dufour, A., Björklund, A., Lindvall, O., Jakobsson, J., and Parmar, M. (2011). Direct conversion of human fibroblasts to dopaminergic neurons. Proc. Natl. Acad. Sci. USA *108*, 10343–10348.

Pircs, K., Nagy, P., Varga, A., Venkei, Z., Erdi, B., Hegedus, K., and Juhasz, G. (2012). Advantages and limitations of different

p62-based assays for estimating autophagic activity in Drosophila. PLoS One *7*, e44214.

Pircs, K., Petri, R., Madsen, S., Brattås, P.L., Vuono, R., Ottosson, D.R., St-Amour, I., Hersbach, B.A., Matusiak-Brückner, M., Lundh, S.H., et al. (2018). Huntingtin aggregation impairs autophagy, leading to argonaute-2 accumulation and global MicroRNA dysregulation. Cell Rep. *24*, 1397–1406.

Poulin, J.F., Zou, J., Drouin-Ouellet, J., Kim, K.Y.A., Cicchetti, F., and Awatramani, R.B. (2014). Defining midbrain dopaminergic neuron diversity by single-cell gene expression profiling. Cell Rep. *9*, 930–943.

Robak, L.A., Jansen, I.E., van Rooij, J., Uitterlinden, A.G., Kraaij, R., Jankovic, J., International Parkinson's Disease Genomics Consortium IPDGC, Heutink, P., and Shulman, J.M. (2017). Excessive burden of lysosomal storage disorder gene variants in Parkinson's disease. Brain *140*, 3191–3203.

Rubinsztein, D.C., Mariño, G., and Kroemer, G. (2011). Autophagy and aging. Cell *146*, 682–695.

Salvador, N., Aguado, C., Horst, M., and Knecht, E. (2000). Import of a cytosolic protein into lysosomes by chaperone-mediated autophagy depends on its folding state. J. Biol. Chem. *275*, 27447–27456.

Sánchez-Danés, A., Richaud-Patin, Y., Carballo-Carbajal, I., Jiménez-Delgado, S., Caig, C., Mora, S., Di Guglielmo, C., Ezquerra, M., Patel, B., Giralt, A., et al. (2012). Disease-specific phenotypes in dopamine neurons from human iPS-based models of genetic and sporadic Parkinson's disease. EMBO Mol. Med. *4*, 380–395.

Schöndorf, D.C., Aureli, M., McAllister, F.E., Hindley, C.J., Mayer, F., Schmid, B., Sardi, S.P., Valsecchi, M., Hoffmann, S., Schwarz, L.K., et al. (2014). iPSC-derived neurons from GBA1-associated Parkinson's disease patients show autophagic defects and impaired calcium homeostasis. Nat. Commun. *5*, 4028.

Shrigley, S., Pircs, K., Barker, R.A., Parmar, M., and Drouin-Ouellet, J. (2018). Simple generation of a high yield culture of induced neurons from human adult skin fibroblasts. J. Vis. Exp. *132*, 56904.

Sposito, T., Preza, E., Mahoney, C.J., Setó-Salvia, N., Ryan, N.S., Morris, H.R., Arber, C., Devine, M.J., Houlden, H., Warner, T.T., et al. (2015). Developmental regulation of tau splicing is disrupted in stem cell-derived neurons from frontotemporal dementia patients with the 10 + 16 splice-site mutation in MAPT. Hum. Mol. Genet. *24*, 5260–5269.

Tang, Y., Liu, M.L., Zang, T., and Zhang, C.L. (2017). Direct reprogramming rather than iPSC-based reprogramming maintains aging hallmarks in human motor neurons. Front. Mol. Neurosci. *10*, 359.

Tiklová, K., Björklund, Å.K., Lahti, L., Fiorenzano, A., Nolbrant, S., Gillberg, L., Volakakis, N., Yokota, C., Hilscher, M.M., Hauling, T., et al. (2019). Single-cell RNA sequencing reveals midbrain dopamine neuron diversity emerging during mouse brain development. Nat. Commun. *10*, 581.

Valenca, G.T., Srivastava, G.P., Oliveira-Filho, J., White, C.C., Yu, L., Schneider, J.A., Buchman, A.S., Shulman, J.M., Bennett, D.A., and De Jager, P.L. (2016). The role of MAPT haplotype H2 and isoform 1N/4R in parkinsonism of older adults. PLoS One *11*, e0157452.

Vuono, R., Winder-Rhodes, S., de Silva, R., Cisbani, G., Drouin-Ouellet, J., REGISTRY Investigators of the European Huntington's Disease Network, Spillantini, M.G., Cicchetti, F., and Barker, R.A. (2015). The role of tau in the pathological process and clinical expression of Huntington's disease. Brain *138*, 1907–1918.

Winder-Rhodes, S.E., Garcia-Reitböck, P., Ban, M., Evans, J.R., Jacques, T.S., Kemppinen, A., Foltynie, T., Williams-Gray, C.H., Chinnery, P.F., Hudson, G., et al. (2012). Genetic and pathological links between Parkinson's disease and the lysosomal disorder Sanfilippo syndrome. Mov. Disord. *27*, 312–315.